CHARACTERIZATION OF AN IMMERSED FINITE RIBBED TUBE USING INVERSE PROBLEM

R. Liétard Université du Havre, LAUE UMR CNRS 6068, Le Havre, FRANCE
D. Décultot Université du Havre, LAUE UMR CNRS 6068, Le Havre, FRANCE
G. Maze Université du Havre, LAUE UMR CNRS 6068, Le Havre, FRANCE

1 INTRODUCTION

Studies on the influence of radial evenly spaced reinforcing ribs on the acoustic scattering from elastic finite cylindrical shells have followed one another over the past decade[1,2,3]. These experimental works, backed up by (i) a theoretical calculation using the thin shell theory and valid for long ribbed cylindrical shells[4], and by (ii) simple diffraction / interference calculations[5], have put the stress on new scattering mechanims due to the periodicity of the ribs. It has been shown that, through these new phenomena (Bragg and Bloch-Floquet diffractions), subsonic surface waves could play a more significant role than that played by supersonic helical waves.

This paper is devoted to the study of a complex object: a finite cylindrical shell, ribbed by a set of periodically spaced internal rings, which represents the central part of more complex structures such as those of submarines. The effects of ribs on the scattering processes are observed in the incidence angle / frequency domain. The rib spacing d and the shell thickness e are estimated, using simple theoretical diffraction / interference equations, from the angular and frequential coordinates of the crossing points between Bragg and Bloch-Floquet experimental trajectories[6].

2 EXPERIMENTAL SETUP

The studied target is a finite cylindrical shell ribbed by a set of 49 evenly spaced internal rings resulting from the machining of a full cylinder made of stainless steel (density ρ = 7900 kg.m^{-3}, longitudinal and transversal velocities C_L = 5790 m.s^{-1} and C_T = 3100 m.s^{-1} respectively). The object present a length L = 75 cm, an outer radius a = 5 cm, and a radius ratio b/a = 0.98 (b inner radius). The ribs are characterized by a thickness l_r = 1 mm, a height h_r = 0.5 cm, and a spacing d = 1.5 cm (Fig. 1). The air-filled target, with extremities closed by disks of the same thickness as that of the shell, is horizontally immersed in water (tank dimensions 30 x 10 x 3 m) where sound velocity is C_{water} = 1470 m.s^{-1}.

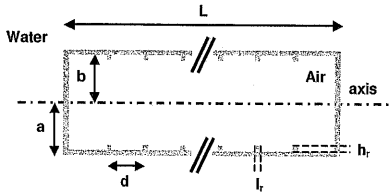

Figure 1: Ribbed shell longitudinal section.
L = 75 cm, a = 5 cm, b/a = 0.98, l_r = 1 mm, h_r = 0.5 cm, d = 1.5 cm.

Experiments are carried out in monostatic configuration[7] (Fig. 2). The acoustic transducer (alternatively used in emission / reception) is oriented in the direction of the center of the shell positioned at 4.5 m. The ribbed target conducts a rotation movement with respect to its main axis: time signals are acquired at one degree intervals from normal incidence ($\alpha = 0°$) to an incidence angle somewhere near axial incidence ($\alpha = 80°$). The emission signal delivered to the broadband Panametrics transducer is one sinusoïd period of frequency 200 kHz ($ka = 42$, k wave number in water). This frequency is chosen in order to respect the 1/75 scale ratio between the studied object and submarines shells. The frequency bandwidth of the emission / reception signal and the half angular aperture of the acoustic beam are plotted on Fig. 3. Given this angular aperture, the target is entirely insonified for each incidence angle.

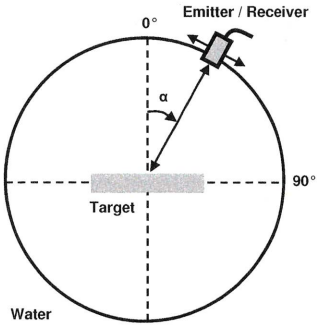

Figure 2: Monostatic configuration.

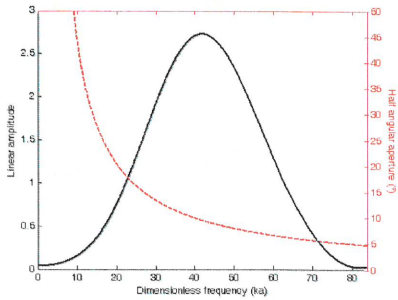

Figure 3: Emission / reception signal bandwidth (black), half angular aperture of the acoustic beam (red).

3 MEASUREMENTS AND DISCUSSION

The experimental spectra, presented in the incidence angle / frequency domain (Fig. 4), are obtained via a Fast Fourier Transform (FFT) performed on time signals for each incidence angle.

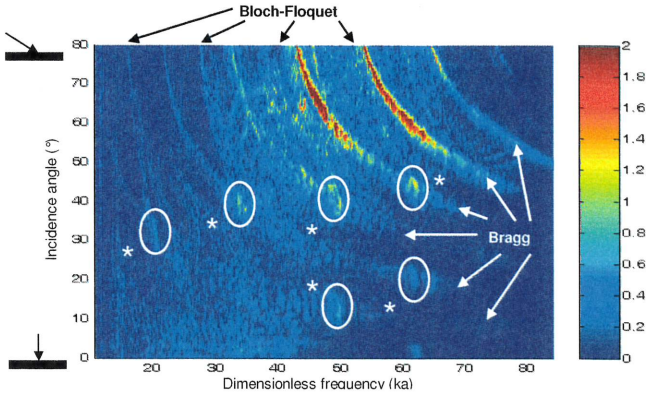

Figure 4: Experimental spectra ($f = 200$ kHz, f emission frequency).

Two phenomena, appearing as trajectories, can be noticed: Bragg and Bloch-Floquet diffractions. Although these phenomena are both related to interferences, their origins are different. Bloch-Floquet diffraction results from the propagation of the axial *A* wave (or A_0^- wave). This subsonic flexural wave, generated on the ribs by the incident wave, scatters each time it meets a rib. The interference of the whole of reemissions gives rise to the phenomenon. Forward Bloch-Floquet waves (BF_{fw}) are distinguished from backward ones (BF_{bw}). These last have a direction of propagation opposite to that given by the projection of the incident wave vector on the shell main axis. Bragg diffraction (BG) is due to the interference of the geometrical reflections of the incident plane wave on the ribs. As a matter of fact, it strongly depends on the rib periodicity. Reinforcements of amplitude at the crossing points between Bloch-Floquet and Bragg trajectories (asterisked * on the Fig. 4) are also observable. Certain characteristics of the ribbed shell, such as the rib spacing *d* and the shell thickness *e*, will thereafter be estimated from the angular and frequential coordinates of these reinforcement points.

A superposition of results from three different calculations is given in Fig. 5. Forward and backward Bloch-Floquet trajectories are evaluated using equations (1) and (2) respectively[5,6]. Bragg trajectories are obtained using equation (3)[5,6]. In all the three calculations, amplitudes are normalized by their maximum values.

$$P_{BF}^{fw} = P_0 \sum_{m=1}^{49} e^{j2\pi fd(m-1)\left(\frac{1}{C_A}+\frac{\sin(\alpha)}{C_{water}}\right)} \quad \text{where} \begin{cases} m=1 \text{ is the index of the insonified rib} \\ 2 \le m \le 49 \text{ is the index of the scatterer rib} \end{cases} \tag{1}$$

$$P_{BF}^{bw} = P_0 \sum_{m=1}^{49} e^{j2\pi fd(m-1)\left(\frac{1}{C_A}-\frac{\sin(\alpha)}{C_{water}}\right)} \quad \text{where} \begin{cases} m=1 \text{ is the index of the insonified rib} \\ 2 \le m \le 49 \text{ is the index of the scatterer rib} \end{cases} \tag{2}$$

$$P_{BG} = P_0 \sum_{m=1}^{49} e^{j\frac{2\pi f}{C_{water}}(m-25)2d\sin(\alpha)} \quad \text{where } m \text{ is the index of the insonified / scatterer rib} \tag{3}$$

In the case of Bloch-Floquet trajectories, phase velocity C_A of the axial *A* flexural wave is calculated beforehand considering a plate in contact with water on one side and with vacuum on the other[8]. In order to take into account the effect of added mass due to the ribs, equation (4) is used to calculate the thickness e_{amr} of this plate.

$$e_{amr} = e + \frac{49 \times h_r l_r}{L} = 1.3 \text{ mm} \quad \text{where } e \text{ is the shell thickness} \tag{4}$$

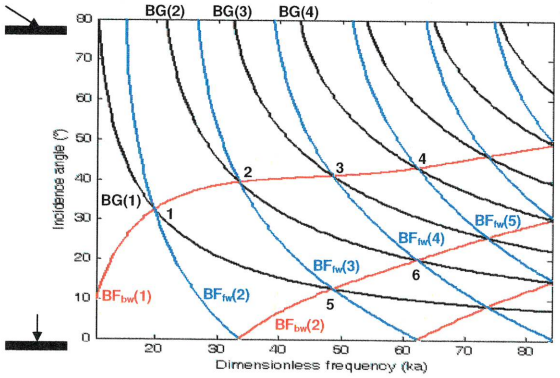

Figure 5: Bragg and Bloch-Floquet theoretical trajectories.

Bragg trajectories and Bloch-Floquet ones (forward and backward) are respectively plotted in black, blue and red, and are numbered by order of appearance (from low frequencies to high ones) knowing that the first forward Bloch-Floquet trajectory is, on these theoretical results, out of range[6]. A good agreement with experimental spectra (Fig. 4) is obtained and the crossing points (also numbered) between the three types of trajectories, points characterized by experimental amplitude reinforcements, are clearly observed.

4 INVERSE PROBLEM

Equations (1) to (3), which allow us to determinate Bragg and Bloch-Floquet trajectories, are sums of the Fraunhoffer type. Thus, with the assumption $P_0 = P_0' = P_0'' = 1$, equations (1), (2) and (3) can respectively be recasted as:

$$\sin(\alpha) = \frac{MC_{water}}{fd} - \frac{C_{water}}{C_A} \tag{5}$$

$$\sin(\alpha) = -\frac{MC_{water}}{fd} + \frac{C_{water}}{C_A} \quad \text{where } M \text{ represents the M}^{th} \text{ trajectory (BG and BF)} \tag{6}$$

$$\sin(\alpha) = \frac{MC_{water}}{2fd} \tag{7}$$

As shown on Fig. 5, trajectories BG(1), $BF_{fw}(2)$ and $BF_{bw}(1)$ meet each other at the first crossing point. Using the three previous equations leads to the following system:

$$\begin{cases} \sin(\alpha) = \dfrac{2C_{water}}{fd} - \dfrac{C_{water}}{C_A} & BF_{fw}(2) \\ \sin(\alpha) = -\dfrac{C_{water}}{fd} + \dfrac{C_{water}}{C_A} & BF_{bw}(1) \\ \sin(\alpha) = \dfrac{C_{water}}{2fd} & BG(1) \end{cases} \tag{8}$$

which can be reduced to

$$\begin{cases} \sin(\alpha) = \dfrac{1}{3}\dfrac{C_{water}}{C_A} \\ f = \dfrac{3}{2}\dfrac{C_A}{d} \end{cases} \tag{9}$$

Thus, using equations from the system above and from the angular and frequential coordinates of the first crossing point, the phase speed C_A of the axial flexural A wave can be estimated at a given frequency and, as a result, the rib spacing d too.

The same mathematical advance is reiterated for the five others crossing points numbered on the Fig. 5. The five resulting reduced equations systems are given below:

$$\begin{cases} \sin(\alpha) = \dfrac{1}{2}\dfrac{C_{water}}{C_A} \\ f = 2\dfrac{C_A}{d} \end{cases} \quad 2^{nd} \text{ crossing point } [BF_{fw}(3), BF_{bw}(1), BG(2)] \tag{10}$$

$$\begin{cases} \sin(\alpha) = \dfrac{3}{5}\dfrac{C_{water}}{C_A} \\ f = \dfrac{5}{2}\dfrac{C_A}{d} \end{cases} \qquad 3^{rd} \text{ crossing point } [BF_{fw}(4),\ BF_{bw}(1),\ BG(3)] \qquad (11)$$

$$\begin{cases} \sin(\alpha) = \dfrac{2}{3}\dfrac{C_{water}}{C_A} \\ f = 3\dfrac{C_A}{d} \end{cases} \qquad 4^{th} \text{ crossing point } [BF_{fw}(5),\ BF_{bw}(1),\ BG(4)] \qquad (12)$$

$$\begin{cases} \sin(\alpha) = \dfrac{1}{5}\dfrac{C_{water}}{C_A} \\ f = \dfrac{5}{2}\dfrac{C_A}{d} \end{cases} \qquad 5^{th} \text{ crossing point } [BF_{fw}(3),\ BF_{bw}(2),\ BG(1)] \qquad (13)$$

$$\begin{cases} \sin(\alpha) = \dfrac{1}{3}\dfrac{C_{water}}{C_A} \\ f = 3\dfrac{C_A}{d} \end{cases} \qquad 6^{th} \text{ crossing point } [BF_{fw}(4),\ BF_{bw}(2),\ BG(2)] \qquad (14)$$

Implementations of equations systems (9) to (14) are carried out for the six crossing points observed on the experimental spectra (Fig. 4). In order to take into account the angular and frequential widths of the crossing points, several couples of coordinates (f,α) have been pointed. Table 1 gathers examples of pointed coordinates and the corresponding estimations of the phase speed C_A and the spacing d.

	Frequency (ka)	Angle α (°)	Amplitude	Phase speed C_A (m.s^{-1})	Spacing d (m)
Crossing point n°1	20.108	33.333	0.629	891.7	0.0142
	20.306	32.163	0.548	920.4	0.0145
	20.504	31.228	0.322	945.1	0.0148
	20.504	29.590	0.335	992.3	0.0155
Crossing point n°3	48.834	41.754	0.900	1324.4	0.0145
	49.429	41.052	0.886	1343.0	0.0145
	50.221	39.415	0.814	1389.1	0.0148
	49.825	38.245	0.803	1424.8	0.0153
Crossing point n°6	61.712	22.105	0.382	1302.1	0.0135
	61.910	20.935	0.370	1371.3	0.0142
	62.108	19.766	0.309	1448.9	0.0150
	62.108	19.298	0.219	1462.7	0.0153

Table 1: Estimations of the phase speed C_A and the spacing d.

The weighted average of all estimated spacings d gives d_{avg} = 1.47 cm, that is to say an error of 2 % with the real rib periodicity (d = 1.5 cm). In the same way, an estimation of the shell thickness using average phase speeds and average frequencies leads to e = 1.18 mm, that is to say a 10 % error with the thickness e_{amr} chosen to plot the theoretical Bloch-Floquet trajectories on Fig. 5. This last estimation is used to recalculate the phase speed of the axial flexural A wave in the case of a plate in contact with water and vacuum. Results are presented on Fig. 6.

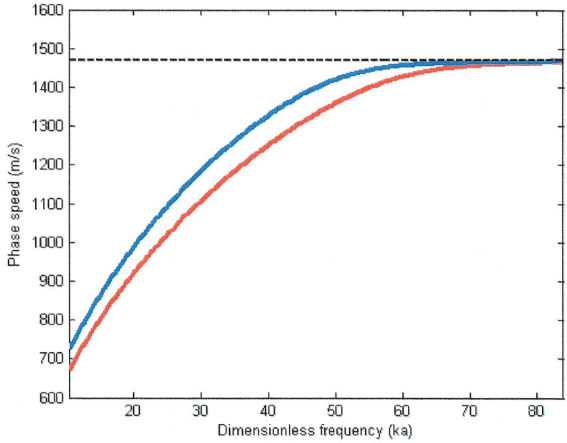

Figure 6: Comparison between calculated (blue) and estimated (red) phase speeds.

Sound velocity in water is plotted in black. The phase speed of the *A* wave used to calculate the theoretical Bloch-Floquet trajectories is plotted in blue. The estimated one is plotted in red. As shown on the figure, there is a good agreement between the two curves. The difference (lower than 100 $m.s^{-1}$ on the frequency range) results from the difficulty to point the experimental crossing points.

5 CONCLUSION

Measurements of the acoustic scattering from a finite cylindrical shell ribbed by a set of periodically spaced rings have been reported. Further information about origins of Bragg and Bloch-Floquet diffractions is provided. It has also been shown that, from the angular and frequential coordinates of amplitude reinforcements experimentally observed, estimations of the rib spacing d and of the shell thickness e_{amr} (taking into account the effect of added mass) could be done. Estimated values have shown a good agreement with the theoretical ones.

6 ACKNOWLEDGEMENTS

The authors are grateful to the Conseil Régional de Haute-Normandie which partly financed this study. They are also grateful to the Director and personnel of the Bassin d'Essais des Carènes de Val de Reuil (France) for allowing them to carry out their experiments under good conditions.

7 REFERENCES

1. D. M. Photiadis, J. A. Bucaro and B. H. Houston, 'Scattering from flexural waves on a ribbed cylindrical shell,' J. Acoust. Soc. Am. 96, 2785-2790. (1994).
2. B. H. Houston, J. A. Bucaro and D. M. Photiadis, 'Broadband acoustic scattering from a ribbed shell,' J. Acoust. Soc. Am. 98, 2851-2853. (1995).
3. D. M. Photiadis, B. H. Houston, E. G. Williams and J. A. Bucaro, 'Resonant response of complex shell structures,' J. Acoust. Soc. Am. 108, 1027-1035. (2000).

4. M. Tran-Van-Nhieu, 'Scattering from a ribbed finite cylindrical shell,' J. Acoust. Soc. Am. 110, 2858-2866. (2001).
5. R. Liétard, D. Décultot, G. Maze and M. Tran-Van-Nhieu, 'Acoustic scattering from a finite cylindrical shell with evenly spaced stiffeners: Experimental investigation,' J. Acoust. Soc. Am. 118, 2142-2146. (2005).
6. R. Liétard, 'Influence de raidisseurs internes régulièrement espacés sur la diffusion acoustique par une coque cylindrique finie immergée: Diffusion de Bragg et diffusion de Bloch-Floquet,' (Influence of evenly spaced internal ribs on the acoustic scattering from an immersed finite cylindrical shell: Bragg scattering and Bloch-Floquet scattering), Thesis. Le Havre, France (2005). in french
7. N. Touraine, L. Haumesser, D. Décultot, G. Maze, A. Klauson and J. Metsaveer, 'Analysis of the acoustic scattering at variable incidences from an extra thin cylindrical shell bounded by hemispherical endcaps,' J. Acoust. Soc. Am. 108, 2187-2196. (2000).
8. A. Grabowska, 'Propagation of elastic wave in solid layer-liquid system,' Archives of Acoustics 4, 1, 57-64. (1979).